Mechanism of the Cell-Penetrating Peptide Transportan 10 Permeation of Lipid Bilayers

Lindsay E. Yandek,* Antje Pokorny,* Anders Florén,† Kristina Knoelke,* Ülo Langel,† and Paulo F. F. Almeida*
*Department of Chemistry and Biochemistry, University of North Carolina Wilmington, Wilmington, North Carolina 28403; and †Department of Neurochemistry, Arrhenius Laboratories, Stockholm University, S-10691 Stockholm, Sweden

ABSTRACT The mechanism of the interaction between the cell-penetrating peptide transportan 10 (tp10) and phospholipid membranes was investigated. Tp10 induces graded release of the contents of phospholipid vesicles. The kinetics of peptide association with vesicles and peptide-induced dye efflux from the vesicle lumen were examined experimentally by stopped-flow fluorescence. The experimental kinetics were analyzed by directly fitting to the data the numerical solution of mathematical kinetic models. A very good global fit was obtained using a model in which tp10 binds to the membrane surface and perturbs it because of the mass imbalance thus created across the bilayer. The perturbed bilayer state allows peptide monomers to insert transiently into its hydrophobic core and cross the membrane, until the peptide mass imbalance is dissipated. In that transient state tp10 "catalyzes" dye efflux from the vesicle lumen. These conclusions are consistent with recent reports that used molecular dynamics simulations to study the interactions between peptide antimicrobials and phospholipid bilayers. A thermodynamic analysis of tp10 binding and insertion in the bilayer using water-membrane transfer hydrophobicity scales is entirely consistent with the model proposed. A small bilayer perturbation is both necessary and sufficient to achieve very good agreement with the model, indicating that the role of the lipids must be included to understand the mechanism of cell-penetrating and antimicrobial peptides.

INTRODUCTION

Cell-penetrating peptides (CPPs), also called protein transduction domains, are a heterogeneous set of peptides that can be broadly divided into two categories: highly cationic and amphipathic. Most peptides investigated belong to the former class. Common examples are penetratin (1), which is a 16-amino acid segment derived for the Antennapedia homeodomain of *Drosophila*, the Tat peptides (2,3), derived from the HIV-1 Tat protein, and simple polyarginine peptides such as $(Arg)_{6-8}$. The transportan 10 (tp10) (4,5) used in this study belongs to the second class. Peptides in this class are similar to antimicrobial (6) and cytolytic or cytotoxic amphipathic peptides. Tp10 is a 21-residue peptide derived from mastoparan, a 14-residue peptide from wasp (*Vespula lewisii*) venom, linked, in a chimeric construct, to a 6-residue sequence from the neuropeptide galanin through an extra lysine residue. Tp10 has been shown to transport cargo across cell membranes (5). The parent transportan, which is slightly longer than tp10, has been reported to transport even larger molecules, such as green fluorescent protein, attached to the peptide by a biotinyl linkage (7). Neither tp10 nor transportan function as ligands for the galanin receptor (4), suggesting that a direct interaction with the lipid bilayer is involved. Transportan (8) and mastoparan X (9,10), which is very similar to the *V. lewisii* mastoparan used in constructing tp10, form amphipathic α-helices when bound to membranes. Therefore, it is very likely that tp10 will also form an α-helix under those conditions. A helical wheel projection of tp10 is shown in Fig. 1. Tp10 contains a high proportion of positively charged amino acids, four lysines, and the N-terminus, and no negative charges, imparting it with a formal $+5$ charge at neutral pH. This charge is large for antimicrobial peptides on a per residue basis. For comparison with some of the best studied amphipathic α-helical antimicrobials, cecropin A (11,12) has a $+7$ charge but 37 residues, magainin-2 (13) has a $+3$ charge and 23 residues, and dermaseptin-1 (14) has a $+4$ charge and 34 residues. Tp10 clearly has the highest charge density of these four peptides. This high charge is a feature in common with the polycationic CPPs. However, in cationic CPPs arginine is more efficient as the basic amino acid than lysine (15). Tp10 contains no arginine but only lysine, which is a common feature of most amphipathic, α-helical, antimicrobial peptides (6).

The mechanism of cell penetration by CPPs was originally believed to be a passive permeation through cell membranes—however unlikely that might have seemed for such highly charged molecules—but more recently most investigators seem to favor the idea that the initial crossing of the plasma membrane occurs by endocytosis. Nevertheless, the problem still remains of how the CPPs exit the endocytic vesicle into the cytoplasm. This has not been resolved. Even the requirement for endocytosis is questionable at this point: many highly charged peptides, especially those rich in arginine, appear to be able to cross hydrophobic media such as bilayers, if these contain anionic lipids or amphiphiles (16). Less clear still is the situation for amphipathic α-helical peptides, antimicrobial or not. δ-Lysin, a 26-residue, amphipathic, α-helical peptide from *Staphylococcus aureus*, was recently proposed to cause dye efflux from phospholipid

Submitted October 31, 2006, and accepted for publication January 10, 2007.

Address reprint requests to Paulo F. F. Almeida, Dept. of Chemistry and Biochemistry, University of North Carolina Wilmington, Wilmington, NC 28403. Tel.: 910-962-7300; Fax: 910-962-3013; E-mail: almeidap@uncw.edu.

0006-3495/07/04/2434/11 $2.00

doi: 10.1529/biophysj.106.100198

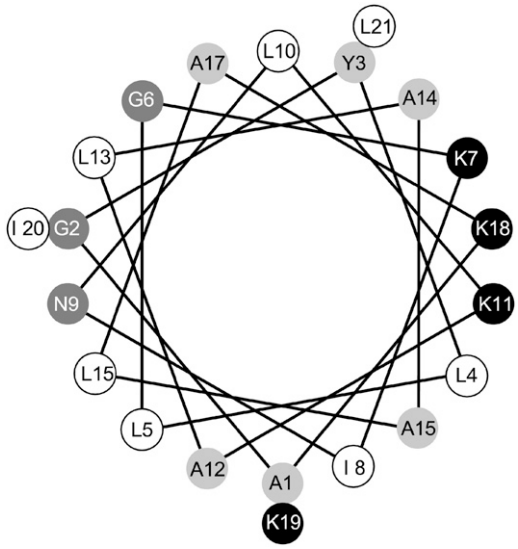

FIGURE 1 Helical wheel projection of Tp10 generated using the program Membrane Protein Explorer (44). Black symbols represent positively charged residues, white, hydrophobic residues, dark gray, hydrophilic (uncharged), and light gray, residues with intermediate polarity. The C-terminus is amidated; therefore it carries no charge.

vesicles by disturbing the membrane, as it crosses the bilayer in the form of a small aggregate, probably a trimer (17,18). This was suggested to occur by a perturbation of the bilayer in the form of a mass imbalance caused directly by the peptide binding to the outer leaflet, possibly resulting in local curvature strain. This perturbation would allow small peptide aggregates to sink deeply into the bilayer and cross it—the so-called 'sinking raft' model (17–19).

Here, a detailed and quantitative analysis of the interaction of tp10 with large unilamellar vesicles (LUVs) of zwitterionic lipids (phosphatidylcholine, PC) and mixtures of PC and the anionic lipid phosphatidylserine (PS) was performed to gain a better understanding of the uptake mechanism of tp10. The experimental data on the kinetics of peptide association with lipid vesicles and the release of encapsulated fluorophores induced by tp10 are consistent with a very simple model. We propose that, similar to δ-lysin, tp10 first associates with the outer leaflet of the bilayer and, by doing so, creates a mass imbalance that disturbs the membrane. We have no evidence for tp10 aggregation. Any cooperative effects appear to be mediated by the lipid: the larger the mass imbalance, the larger the bilayer perturbation. At some point, the tp10 peptides simply cross the bilayer, allowing efflux of entrapped dye to occur concomitant with that process. The results are discussed in light of recent molecular dynamics simulations (20–22), which show antimicrobials crossing a bilayer by a very similar mechanism. The likelihood of this mechanism is assessed based on thermodynamic calculations of peptide transfer, first to the bilayer interface and then to its hydrophobic core, using the approach of White and Wimley (23).

MATERIALS AND METHODS

Chemicals

1-Palmitoyl-2-oleoyl-*sn*-glycero-3-phosphocholine (POPC) and 1-palmitoyl-2-oleoyl-*sn*-glycero-3-phosphoserine (POPS) in chloroform solution were purchased from Avanti Polar Lipids (Alabaster, AL). 8-Aminonaphtalene-1,3,6-trisulfonic acid, disodium salt (ANTS) and p-xylene-bis-pyridinium bromide (DPX) were purchased from Molecular Probes/Invitrogen (Carlsbad, CA). Carboxyfluorescein (99% pure, lot A015252901) was purchased from ACROS (Morris Plains, NJ). 7-Methoxycoumarin-4-acetic acid was from Sigma-Aldrich (St. Louis, MO). Anisole was purchased from Aldrich and thioanisole from Alfa Aesar (Ward Hill, MA). Trifluoroacetic acid (TFA) was from Mallenckrodt (Phillipsburg, NJ). Organic solvents (high-performance liquid chromatography (HPLC)/American Chemical Society (ACS) grade) were purchased from Burdick & Jackson (Muskegon, MI). Lipids and probes were tested by thin-layer chromatography and used without further purification. Amino acids and activators used in the preparation of the first batch of tp10 were purchased from Neosystems (Strasbourg, France). Fmoc-protected amino acids and resins used in the second batch of tp10 were obtained from EMD Biosciences (San Diego, CA).

Preparation of tp10

Standard tp10 (AGYLLGKINLKALAALAKKIL-amide) was synthesized using solid-state synthesis, as described before (4). For the fluorescent derivatives, the backbone of tp10 was synthesized in a 0.1-mmol scale on an Applied Biosystems (Foster City, CA) Model 431A peptide synthesizer on solid support, using dicyclohexyl-carbodiimide (DCC)/hydroxybenzotriazole (HOBt) activation strategy. Standard t-Boc amino acids were coupled as HOBt esters to a p-methylbenzylhydrylamine (MBHA) resin to obtain C-terminal amidation. At position Lys-7 we used t-bocLys (Fmoc) to be able to selectively label the amino group at the side chain. After the synthesis the Fmoc group was removed with 10% piperidine, and three equivalents of 7-methoxycoumarin-4-acetic acid were coupled manually using HOBt- and o-benzotriazole-1-yl-*N*,*N*,*N*′,*N*′-tetramethyluronium tetrafluorborate (TBTU). This coupling procedure was repeated three times. The peptide was then cleaved from the resin with hydrogen fluoride using 10% paracreosol as scavenger (30 min, 0°C), extracted with ether, and lyophilized. From the crude product both 7-methoxycoumarin-tp10 (tp10-7mc) and unlabeled tp10 could be isolated by preparative HPLC in roughly equal amounts. Both products were further purified by semipreparative HPLC. The purity of the peptides was >99% as checked by HPLC analysis on Nucleosil 1203 C18 column (0.4 cm × 10 cm). The molecular mass of each peptide was determined on a matrix-assisted laser desorption ionization-time of flight mass spectrometer (Voyager STR, Applied Biosystems, Foster City, CA).

An additional batch of tp10 was synthesized, also by solid phase Fmoc chemistry, on a 0.1-mmol scale using a PS3 Peptide Synthesizer (Protein Technologies, Tucson, AZ). Double couplings were used for leucine, isoleucine, valine, and tyrosine. Peptide cleavage and removal of side-chain protecting groups was achieved by stirring 10 mL TFA, 0.5 mL water, 0.5 mL anisole, and 0.5 mL thioanisole at room temperature for 2 h. After precipitation with methyl-tert-butyl ether (OmniSolv, EMD Biosciences, San Diego, CA), the peptide was dissolved in 10 mL of 10% acetic acid. The peptides were then purified by reversed-phase HPLC on a C18 column (Vydac, Hesperia, CA) with an acetonitrile/water gradient (25%–50% acetonitrile over 50 min) with 0.1% TFA and lyophilized. Peptide purity and mass was confirmed with electrospray-ionization time-of-flight mass spectrometry.

Preparation of large unilamellar vesicles

LUVs were prepared by mixing the appropriate lipid amounts in chloroform in a round-bottom flask. The solvent was rapidly evaporated using a rotary evaporator (Büchi R-3000, Flawil, Switzerland) at 60°C–70°C. The lipid film was then placed under vacuum for 4–8 h and hydrated by the addition of buffer containing 20 mM MOPS (3-(*N*-morpholino)propanesulfonic acid),

pH 7.5, 0.1 mM EGTA, 0.02% NaN_3, and 100 mM KCl or appropriately modified as indicated below. The suspension of multilamellar vesicles was subjected to five freeze-thaw cycles to increase the degree of dye (carboxyfluorescein (CF) or ANTS/DPX) encapsulation. The suspension was then extruded 10 times through two stacked Nuclepore polycarbonate filters (Whatman, Florham, NJ) of 0.1-μm pore size, using a water-jacketed high pressure extruder from Lipex Biomembranes (Vancouver, Canada) at room temperature. Lipid concentrations were assayed by the Bartlett phosphate method (24), modified as previously described (17), with the absorbance read at 580 nm.

Kinetics of tp10/bilayer association

The kinetics of association of tp10-7mc with LUVs of POPC and POPS/POPC 2:8, as a function of lipid concentration, were recorded in a Applied Photophysics (Leatherhead, Surrey, UK) SX.18MV stopped-flow fluorimeter. The excitation was at 350 nm and the emission was recorded through a long-pass filter GG 385 (Edmund Industrial Optics, Barrington, NJ). The emission maximum of tp10-7mc (as that of the fluorophore itself) is 396 nm. The peptide concentration was 0.5 μM (after mixing). Lipid concentrations varied between 5 and 400 μM (after mixing).

ANTS/DPX assay

Steady-state fluorescence measurements were performed in an SLM-Aminco 8100 spectrofluorimeter (Urbana, IL). In the ANTS/DPX assay, which was performed as described in detail by Ladokhin et al. (25) and Ladokhin et al. (26), excitation was at 365 nm (8 nm slitwidth) and emission was at 515 nm (16 nm slitwidth). The solution encapsulated in the LUVs contained ANTS/DPX (5 mM each), 20 mM MOPS, pH 7.5, 0.1 mM EGTA, 0.02% NaN_3, and 70 mM KCl. The titrating solution contained 45 mM DPX, 20 mM MOPS, pH 7.5, 0.1 mM EGTA, 0.02% NaN_3, and 30 mM KCl. After extrusion, the LUVs with encapsulated ANTS and DPX were passed through a Sephadex-G25 column to separate the dye in the external buffer from the vesicles.

Carboxyfluorescein efflux experiments

LUVs for CF efflux kinetics measurements where prepared by hydration of the lipid film in 20 mM MOPS buffer, pH 7.5, containing 0.1 mM EGTA, 0.02% NaN_3, and 50 mM CF, to give a final lipid concentration of 10 mM. For fluorescence measurements, the suspension was diluted to the desired lipid concentration in buffer containing 20 mM MOPS, pH 7.5, 100 mM KCl, 0.1 mM EGTA, and 0.02% NaN_3, which has the same osmolarity as the CF-containing buffer. After extrusion, fluorophore-containing LUVs were passed through a Sephadex-G25 column to separate the dye in the external buffer from the vesicles. The kinetics of carboxyfluorescein efflux, measured by the relief of self-quenching of CF fluorescence, was recorded in a Applied Photophysics SX.18MV stopped-flow fluorimeter. The excitation was at 470 nm and the emission was recorded through a long-pass filter GG 530 (Edmund Industrial Optics). The peptide concentration was 0.5 μM in all experiments. The final fraction of CF release was determined by comparison of the fluorescence with that obtained by addition of Triton-X-100, which dissolves the vesicles and releases all the dye.

Theoretical models and analysis of dye efflux kinetics

The association and dissociation kinetics of tp10 monomers in aqueous solution with lipid vesicles can be described by the scheme,

$$M_w + L \underset{k_{off}}{\overset{k_{on}}{\rightleftharpoons}} M_L^o, \tag{1}$$

where M_w are tp10 monomers in water, L represents lipid vesicles, and M_L^o represent monomers bound to the outer leaflet of the membrane. The corresponding differential equations,

$$\frac{dM_w}{dt} = -k_{on}M_w[L] + k_{off}M_L^o \tag{2}$$

$$\frac{dM_L^o}{dt} = k_{on}M_w[L] - k_{off}M_L^o, \tag{3}$$

have the solution

$$M_w(t) = \exp(-k_{app}t), \tag{4}$$

where

$$k_{app} = k_{on}[L] + k_{off}. \tag{5}$$

In these equations, $[L]$ is the vesicle concentration, but it will always be expressed in terms of lipid concentration (1 LUV $\simeq 10^5$ lipids). Because the number of peptides bound per vesicle is always small and vesicles do not disappear when peptides bind, $[L]$ is considered constant in the calculations.

The experimental data of CF efflux kinetics were analyzed with the model depicted in Fig. 2. This is similar to the model used for δ-lysin (18) but simpler because only monomers are involved. In this model, the peptides bind to the membrane surface and the increased mass of the outer leaflet results in bilayer perturbation, possibly through local curvature strain. This strain is relieved by the peptides inserting into and crossing the bilayer, after which those that crossed remain mostly associated with the inner leaflet of the bilayer. That is, desorption from the inner leaflet into the vesicle interior is not included in the scheme because of the comparatively small magnitudes of the off-rate constants. The translocation process continues until the concentrations of the peptide on both sides of the membrane are approximately equal. The efflux of CF is in this way 'catalyzed' by the inserted peptide state, which corresponds to the largest bilayer perturbation.

This model was translated into a set of coupled differential equations, which constitute the kinetic model. The following scheme involves only tp10 monomers but was appropriately modified to include possible aggregates in other variants. In these equations, M_L^o and M_L^i represent monomers bound to the outer and inner leaflets of the bilayer, respectively, and M_L^m represent tp10 monomers inserted into the hydrophobic core of the membrane. According to the model, this species correlates with dye efflux, induced transiently as the peptide monomer crosses the bilayer (Eq. 9).

Membrane species:

$$\frac{dM_L^o}{dt} = k_{on}M_wL - k_{off}M_L^o - k_{ins}M_L^o + k_{dins}M_L^m \tag{6}$$

$$\frac{dM_L^m}{dt} = k_{ins}(M_L^o + M_L^i) - 2\,k_{dins}M_L^m \tag{7}$$

$$\frac{dM_L^i}{dt} = -k_{ins}M_L^i + k_{dins}M_L^m \tag{8}$$

Carboxyfluorescein efflux:

$$\frac{d\mathrm{CF}_{out}}{dt} = k_{eflx}(1 - \mathrm{CF}_{out})M_L^m/(v_oL) \tag{9}$$

The apparent rate 'constant' for insertion k_{ins} depends on the difference in the concentrations of peptide bound to the outer and inner leaflets of the lipid bilayer,

$$k_{ins} = k_{ins}^* \times |[P]_{outer} - [P]_{inner}|, \tag{10}$$

where $[P]_{outer}$ and $[P]_{inner}$ are the concentrations, on the membrane, of peptides bound to the outer and inner leaflets of the bilayer. Unlike k_{ins}, the rate constant k_{ins}^* is a true constant. The rate constant for the reverse of insertion is k_{dins}. All concentrations of peptide species indicated by expressions of the type M_x, whether referring to solution species or membrane-bound species, are expressed relative to the total aqueous solution volume. The factor $v_o = 0.6/2$ is about half the specific molar volume of the hydrophobic portion of a lipid ($\sim 0.6\,M^{-1}$), assumed of $\simeq 15\,Å \times 70\,Å^2$. Division by 2 corrects $[L]$ for the two

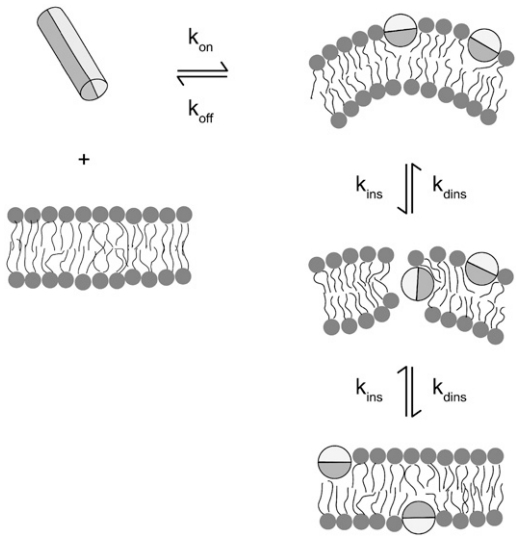

FIGURE 2 Scheme of the model for peptide-induced transient pore formation and peptide translocation across the lipid bilayer. The α-helices are shown as cylinders (in *cross section* on the *right*), where the darker half-circles represent the hydrophobic faces and the lighter half-circles represent the hydrophilic faces. Also indicated are the apparent rate constants for each process. The mathematical translation of this scheme is given by Eqs. 2, 3, and 6–10. Binding of peptides creates a mass imbalance across the lipid bilayer, which perturbs the membrane, possibly because of increase in local curvature strain. This perturbation enhances the probability of a peptide transiently inserting into the bilayer hydrophobic core and eventually crossing the bilayer. In the bilayer-inserted state, the peptide catalyzes dye efflux from the vesicle lumen; this state constitutes the apparent 'pore'. As peptide translocation is completed, the mass balance across the bilayer is restored and the rate of efflux becomes very slow or eventually stops.

leaflets of the lipid bilayer. For example, the concentration of bound monomer relative to the lipid is $m_o = M_o/(v_oL)$, M_o being its concentration relative to water. The peptide concentrations indicated by expressions of the type $[P]_x$ are expressed relative to the lipid, not to water.

For the reverse experiment, an additional block of equations was added, corresponding to the initial state in the donor vesicles preequilibrated with tp10. This block is similar to the block corresponding to tp10 association to vesicles (Eqs. 6–8 above). The initial conditions were calculated, from the integrated equations in the forward reaction setting the time to 1 h, which was the preincubation time of tp10 with empty vesicles.

Two mechanisms can be envisaged for the release of dye from the vesicles, graded or all-or-none (25,26). Because in the graded mechanism partially empty vesicles also contribute to the fluorescence, especially at later times, the theoretical kinetic curves of carboxyfluorescein efflux were corrected for this effect as described in detail before (18). This correction changes the calculated curves slightly, with minor effects on the fit parameters.

The sets of differential equations describing the model were solved by numerical integration with a fifth-order Runge-Kutta method with constant step size (27). The numerical solution was fit directly to the experimental data with a simplex algorithm (27). In the analysis of carboxyfluorescein efflux, the on-rate constants, k_{on}, obtained for the binding kinetics, were used as fixed parameters. The off-rate constants, k_{off}, were allowed to vary because of great uncertainty in their determination from the intercept of the plot of the apparent rate constant against lipid concentration in the binding kinetics. Of the remaining four rate constants (including k_{off}), only three were allowed to vary because k_{eflx} and k_{dins} show a very large mutual correlation effect. We thus fixed k_{eflx} at an average value. The other three constants, k_{off}, k_{ins}, and k_{dins}, were adjusted by a global fit to all data sets of different lipid compositions. This global fit was performed in two stages. First, a simultaneous fit to all data for POPC and POPC/POPS (separately) vesicles was performed. Then, a 50% variation was allowed on each of the three constants and the curves were fit individually. The mean values of the individual fits were then used as a new global fit and the refinement step was repeated. The final values are given in Table 1. In addition, an amplitude factor (0.75–1.2) was allowed for each curve. This corrects for any experimental error in the determination of the maximum dye release.

RESULTS

Tp10 aggregation in solution

Tp10 does not contain an intrinsic fluorophore, such as tryptophan. Therefore, tp10-7mc, a version of tp10 modified with the fluorophore 7-methoxycoumarin-4-acetic acid was used to examine peptide aggregation in solution and the kinetics of binding to membranes. In this tp10-7mc, the fluorophore is attached to the ϵ-amino group of Lys-7 of tp10 through an amide bond to the acetic acid group of the coumarin. As shown in the next section, a decrease in fluorescence intensity is observed when tp10-7mc binds to membranes. For dilute solutions in which the peptides exist as monomers, the fluorescence intensity should be a linear function of concentration. If the peptide concentration is increased, the equilibrium between monomers and possible aggregates will be shifted toward the aggregated state. The fluorescence intensity may then be expected to change if the fluorophore is exposed to a different environment as a consequence of oligomerization or aggregation.

We find that the intensity of fluorescence emission of 7-methoxycoumarin at its maximum (396 nm) is a perfect linear function of the tp10-7mc concentration between 0.04 and 40 μM (Fig. 3). This is consistent with the existence of only one species of tp10-7mc in aqueous solution. Of course, it does not prove that no aggregation takes place, because the fluorophore could be always exposed to water if small oligomers occur. However, because tp10-7mc must almost certainly be a monomer at the low end of the concentration range examined (0.04 μM), it is probably monomeric throughout this concentration range. It appears unlikely that no fluorescence change would occur upon oligomerization because a decrease in coumarin fluorescence does occur upon binding to membranes, indicating that the fluorophore is sensitive to environment. In the next section we present

TABLE 1 Rate constants obtained from the fits of experimental kinetics to the model. The error is estimated from the fits using the linear regression (on-rates) or the variance in fitting the individual curves (all other constants), as described in Materials and Methods

	POPC	POPS/POPC 2:8
k_{on}	$(7.4 \pm 0.5) \times 10^4$ $M^{-1}s^{-1}$	$(2.6 \pm 0.08) \times 10^5$ $M^{-1}s^{-1}$
k_{off}	1.5 ± 0.4 s^{-1}	2.4 ± 0.3 s^{-1}
k^*_{ins}	2.2 ± 0.9 $M^{-1}s^{-1}$	1.4 ± 0.5 $M^{-1}s^{-1}$
k_{dins}	0.40 ± 0.15 s^{-1}	0.26 ± 0.05 s^{-1}
k_{eflx}	5.0 $M^{-1}s^{-1}$	5.0 $M^{-1}s^{-1}$

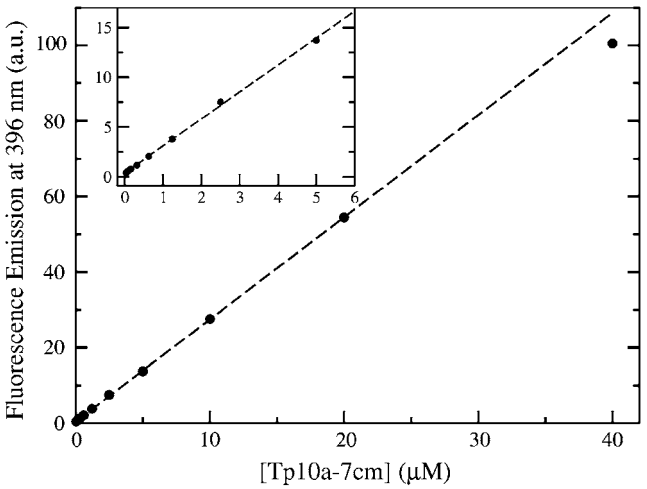

FIGURE 3 Fluorescence of tp10-7mc as a function of its concentration in aqueous solution. The experiment was performed by serial dilution of the same solution. The inset shows the lower concentrations. Only perhaps at ~40 μM is there a slight deviation from the linear dependence.

further evidence that tp10 exists predominantly in a monomeric state in water. Because tp10-7mc (+4 charge) has one less positive charge than tp10 (+5), we expect tp10 to have even a greater tendency to be monomeric in aqueous solutions. Cecropin A, for example, which has a smaller charge density, +5/37 residues compared to tp10 with +5/21 residues, is known to be monomeric in solution at a concentration of 26 μM (28).

Kinetics of tp10 association with phospholipid bilayers

The rates of association and dissociation of tp10-7mc with phospholipid vesicles of POPC and POPS/POPC 2:8 were measured at room temperature (~22°C) by monitoring the rate of change in fluorescence emission upon excitation of the coumarin moiety at 350 nm by stopped-flow fluorescence. When tp10-7mc binds to phospholipid vesicles a decrease in fluorescence emission recorded through a 385-long-pass filter is observed. This decrease in fluorescence intensity was used to monitor the association kinetics of tp10-7mc with LUVs. In most cases the curves of fluorescence intensity as a function of time were well fit by a single exponential decay (Fig. 4, *A*, POPC, and *B*, POPS/POPC 2:8), in accordance with Eq. 4,

$$M_w(t) = \exp(-k_{app}t).$$

That the kinetics of association are exactly described by a single exponential function further supports the assumption that tp10 exists only as a monomer in aqueous buffer, pH 7.5, at the peptide concentrations used in this work.

If a mixed population of monomers and oligomers existed, it is very unlikely that they all would associate with the LUVs with the same rate constants, so that a multiexponential decay would probably be observed. The apparent rate constant,

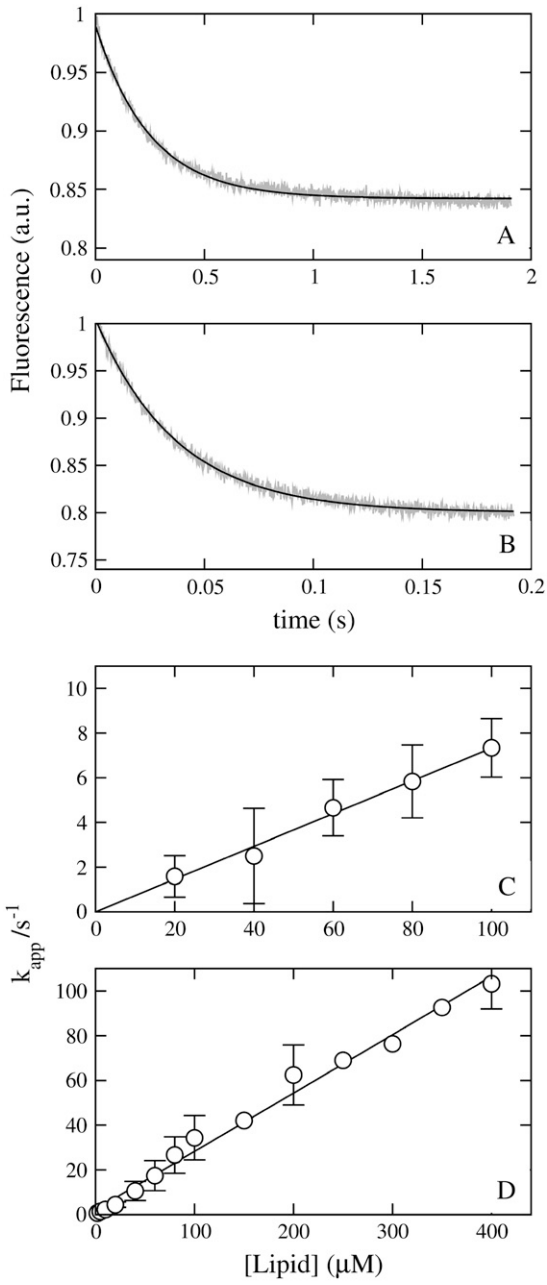

FIGURE 4 Binding kinetics of tp10-7mc to LUVs of POPC (*A* and *C*) and POPS/POPC 2:8 (*B* and *D*). The experimental decay of the fluorescence of tp10-7mc (7-methoxycoumarin chromophore) upon mixing with LUVs to a final lipid concentration of 80 μM is shown for POPC (*A*) and POPS/POPC 2:8 (*B*). The lines are single exponential fits (Eq. 4). Note that the timescale varies by a factor of 10 between the two types of vesicles. A plot of the apparent values of the rate constant in experiments such as those in (*A*) and (*B*), as a function of lipid concentration is shown for POPC (*C*) and POPS/POPC 2:8 (*D*). The values of the slopes correspond to k_{on} (Eq. 5), which are indicated in Table 1. Two samples were examined for POPC and three samples for POPS/POPC 2:8. For each sample, 3–5 curves were collected. The means and standard deviations from all values are shown. The major contribution to the variance arises from the different samples. When not shown, the standard deviation is inside the point, but most of these cases correspond to concentrations examined on the same sample.

k_{app}, determined from the fits is plotted as a function of the lipid concentration in Fig. 4, *C* (POPC) and *D* (POPS/POPC 2:8) to obtain the on-rate constants (k_{on}), according to Eq. 5. The values obtained were $k_{on} = 7.4 \times 10^4\ M^{-1}s^{-1}$ for POPC and $k_{on} = 2.6 \times 10^5\ M^{-1}s^{-1}$ for POPS/POPC 2:8 (Table 1). The latter is at the diffusion limit, unlike for POPC LUVs. In the case of POPS:POPC 2:8 vesicles, the curves of fluorescence intensity as a function of time were well fit by a single exponential decay for lipid concentrations >60 μM (Fig. 4 *B*). Below 60 μM, however, two exponentials were required to fit the curves. This may indicate that at low lipid concentration the peptide can partially discriminate between bilayer areas rich in PS and binds to those areas faster. However, analysis of the curves corresponding to 20–60 μM lipid with a single exponential, which does not fit very well, or using the average of the apparent time constants ($1/k_{app}$) obtained from a two-exponential fit yields the same apparent constant (k_{app}). Extrapolation of the straight lines to zero to obtain k_{off} has too much uncertainty because the intercept occurs very close to the zero of the ordinate. Therefore, k_{off} was left as a free parameter and determined from the fits to CF efflux kinetics. There, a value of $k_{off} \sim 2\ s^{-1}$ was obtained for both types of vesicles, POPC and POPS/POPC 2:8, within experimental error. The value of $k_{off} \sim 2\ s^{-1}$ is actually what is also obtained from the fit of k_{app} versus lipid concentration shown in Fig. 4 *D*.

Mechanism of dye release from vesicles: all-or-none or graded?

The ANTS/DPX assay (25,26) was used to determine whether the mode of dye release from lipid vesicles by tp10 is 'all-or-none' or graded. In this assay, a fluorophore, ANTS, is encapsulated in the vesicles together with a fluorescence quencher, DPX. The quenching of ANTS fluorescence by DPX is a bimolecular process, therefore strongly dependent on quencher concentration. Peptide interaction with the vesicle causes the release of both fluorophore and quencher. The increased ANTS fluorescence originating from ANTS that escaped to the external medium is titrated by adding additional quencher (DPX). The resulting fluorescence is then only due to ANTS remaining in the vesicles, where it is inaccessible to externally added DPX. If the release were all-or-none, the degree of quenching in the vesicles would be independent of the amount ANTS and DPX released, since the vesicles would be either all empty or completely intact. Only the intact vesicles would contribute to the signal after the external quencher was added, and since the DPX concentration in those intact vesicles does not change, neither does the degree of quenching. However, if the release is graded, only part of the fluorophore is released along with the quencher. The fluorescence of ANTS remaining in the vesicles increases because the quencher concentration has also been lowered due to partial release. The degree of quenching will then become a function of the amount of ANTS and DPX released. As shown in Fig. 5, in the case of tp10 the mode of release of vesicle contents is clearly graded. The dashed line would correspond to all-or-none release. The data in Fig. 5 were corrected for incomplete entrapment (26). The solid line on the figure is Eq. 11 (25),

$$Q_{in} = \frac{F_i}{F_i^{max}} = \frac{1}{(1 + K_d[DPX]_0(1 - f_{out})^{\alpha})(1 + K_a[DPX]_0(1 - f_{out})^{\alpha})}, \quad (11)$$

where F_i and F_i^{max} are the fluorescence intensities from the vesicle interior with and without quencher (DPX), $[DPX]_0$ is the initial concentration encapsulated (5 mM was used for both ANTS and DPX), f_{out} is the ANTS fraction outside the vesicles, $K_d = 50\ M^{-1}$ (25) is the dynamic quenching constant, $K_a = 180\ M^{-1}$ (best fit value) is the static quenching constant, and $\alpha = 0.55$ (best fit value) is the ratio of the rates of release of DPX to ANTS, which indicates that ANTS efflux is about twice as fast as DPX efflux.

Carboxyfluorescein efflux kinetics: forward and reverse

Carboxyfluorescein is self-quenched at high concentrations. Addition of peptide to phospholipid vesicles containing CF encapsulated at high concentration causes dye efflux and consequent increase in fluorescence, arising mainly from the dye that escaped from the vesicle lumen. A small effect arising from relief of self-quenching of CF inside the vesicle also occurs and was taken into account in this analysis (18). The rate of CF fluorescence increase is used to follow the

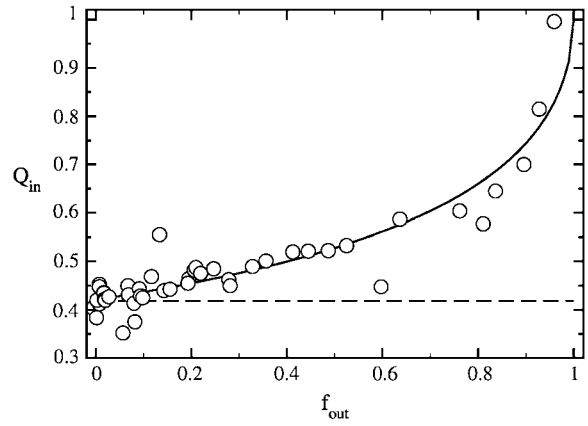

FIGURE 5 ANTS/DPX assay to determine the mechanism of release. The quenching function inside, $Q_{in} = F_i/F_i^{max}$, which is the ratio of ANTS fluorescence inside the vesicle in the presence (F_i) and absence (F_i^{max}) of quencher (DPX), is plotted against the ANTS fraction outside the vesicles, f_{out}, corrected for incomplete entrapment as described in Ladokhin et al. (26). The horizontal line would be the result expected for an all-or-none release. Clearly, release is graded. The solid line represents a fit of Eq. 11 to the data points, which are pooled from three independent samples. The fit parameters are $K_d = 50\ M^{-1}$, $K_a = 180\ M^{-1}$, and $\alpha = 0.55$.

kinetics of dye efflux. Tp10 at a final concentration of 0.5 μM was mixed with LUVs, varying the lipid concentration between 20 and 200 μM (after mixing), and the kinetics of dye efflux were monitored. The maximum possible fluorescence levels were determined by adding the detergent Triton X-100 to the vesicle suspension at a concentration of 1%, which dissolves the vesicles.

The kinetics of dye release obtained by adding the peptides from aqueous solution are not very sensitive to the backward rates, that is, the rate constants in the direction of the reaction written as the reverse of the scheme shown in Fig. 2, such as the off-rates from the vesicles. To better determine those rates, a 'reverse experiment' was carried out: the efflux kinetics were measured after tp10 was prebound for 1 h to empty (donor) vesicles, which were mixed in the stopped-flow with acceptor vesicles containing CF. Now, tp10 must dissociate from the donor vesicles back into water before being able to bind to acceptor vesicles and induce CF release. Both types of vesicles (donors and acceptors) had the same lipid composition. These experiments were performed both with pure POPC (Fig. 6, *A*, forward, and *B*, reverse) and with POPS/POPC 2:8 vesicles (Fig. 7, *A*, forward, and *B*, reverse). We note, first, that for the same final lipid concentration (50 μM) the timescale for dye release in the reverse reaction is only $\sim$10$\times$ longer than in the forward reaction, indicating that tp10 readily desorbs from the donor vesicles and equilibrates over the entire vesicle population. Second, the difference between the kinetics of efflux from POPS/POPC 2:8 and pure POPC is not very significant. This is true despite the +5 charge carried by tp10 at pH 7.5, which is expected to lead to stronger binding to the vesicles containing the anionic lipid POPS—as indeed it does, which is shown by a k_{on} $\sim$10$\times$ larger than for POPC LUVs. In both cases, but more pronounced for POPS/POPC 2:8 vesicles, the kinetics of CF efflux and the final amount of dye released depend on lipid concentration. The lines shown in Figs. 6 and 7 are the best global fits of the theoretical model (Eqs. 2, 3, and 6–11) to the two data sets. Forward and reverse kinetics for POPC are described by one set of parameters and the same is true for POPS/POPC 2:8, with parameters that are only slightly different from those used for POPC, except for the on-rate constant. These fits are analyzed in more detail in the next section.

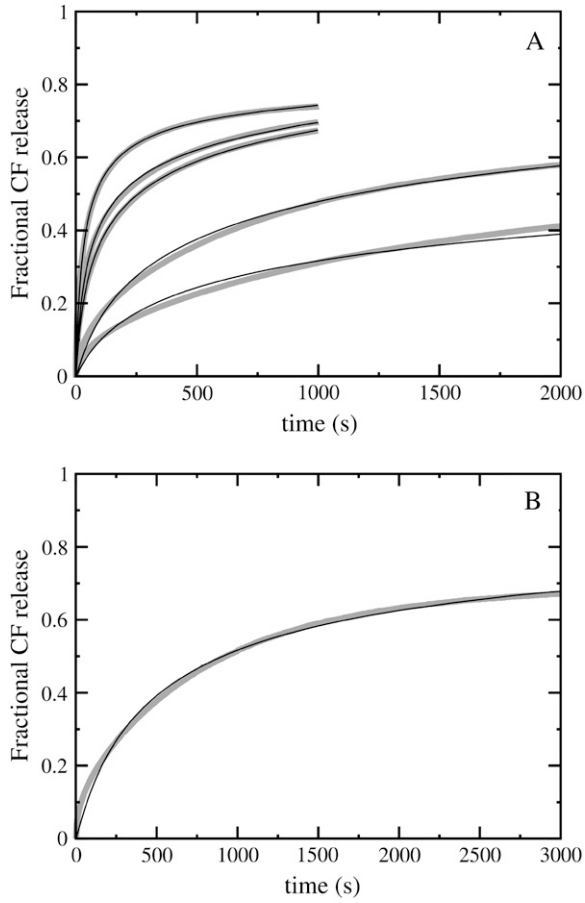

FIGURE 6 (*A*) Kinetics of carboxyfluorescein efflux from POPC LUVs after tp10 (0.5 μM) addition. The gray curves, from top (fastest) to bottom (slowest) are the experimental data for 20, 30, 50, 100, and 200 μM lipid. The data were normalized by the Triton X-100 release levels. Each curve is the average of a total of 5–9 experiments performed on 2 or 3 independent samples. The thin black lines represent the best fit of the theoretical kinetic model to the experimental data, allowing for a 50% variation in each parameter relative to the best simultaneous fit. The values of the best global fit are indicated in Table 1. Because Triton X-100 release levels obtained with this peptide have shown a significant variation between different preparations, an amplitude factor of 0.75–1.2 was included in the fits. For the fits shown, the amplitude factors are 0.83, 0.97, 1.2, 1.2, and 1.2 for 20, 30, 50, 100, and 200 μM lipid, respectively. (*B*) Reverse experiment of carboxyfluorescein efflux from POPC LUVs induced by tp10. Donor vesicles were prepared by preincubating 1 μM tp10 with 60 μM POPC (empty LUVs) for 1 h, and the kinetics were followed by mixing with 40-μM POPC acceptor vesicles (containing dye) so that the final concentration of POPC was 50 μM and the final tp10 concentration was 0.5 μM in the stopped-flow experiment. The efflux fraction is normalized to the Triton X-100 release level. The amplitude factor was 0.92. The gray curve represents the experimental data, and the thin black line is the best (global) fit, with the same parameters as in (*A*), within the allowed variation (Table 1). Please note that the timescales are different in panels (*A*) and (*B*).

Analysis of efflux kinetics

The on-rate constants for tp10 association with lipid vesicles were determined from the binding kinetics and fixed in the remaining fits. For the other parameters, separately for POPC and POPS/POPC 2:8, the best global fit was sought that would describe both the lipid concentration dependence of the forward CF-efflux kinetics (Figs. 6 *A* and 7 *A*) and the reverse kinetics (Figs. 6 *B* and 7 *B*). The values that yielded the best fits for the model proposed (Fig. 2) are listed in Table 1. For the definition of the rate constants, please refer to Fig. 2 and Eqs. 6–11, which describe the kinetic model. Other models were also tried. Models that require dimerization or tetramerization on the membrane, with the dimer or tetramer as the state that translocates across the bilayer, were able to fit quite well the kinetics of tp10 interaction with vesicles of POPS/POPC 2:8. However, though the dimer

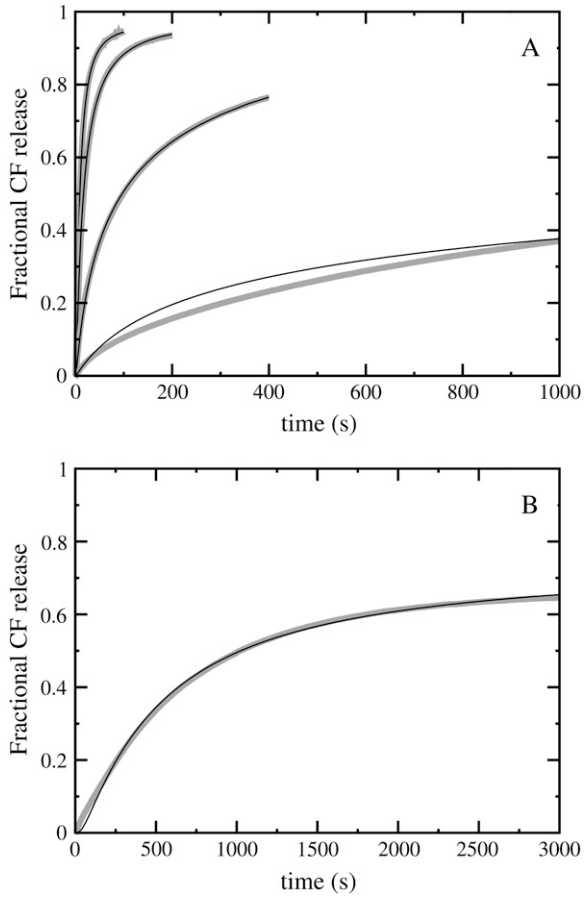

FIGURE 7 Same as for Fig. 6, but for vesicles of POPS/POPC 2:8. (*A*) Forward reaction. The peptide concentration is 0.5 μM and the lipid concentrations are 20, 30, 50, and 100 μM. The amplitude factors are 0.97, 0.98, 1.2, and 1.2, in the same order. (*B*) Reverse experiment. The amplitude factor is 0.75. Please note that the timescales are different in panels (*A*) and (*B*).

model can fit the POPC data, it does so worse than the monomer model. We cannot, of course, discard the possibility that the oligomerization state of the peptide species that crosses the bilayer is different in POPC and POPS/POPC 2:8. In any case, overall none of these models is better than the one involving only monomers, which is the simplest. Another model tried was a simple perturbation of the membrane by surface-associated peptides, but this did not yield good fits. For the simple model proposed, which involves only monomers, it is possible to obtain excellent fits for each curve. The requirement that the model fit the reverse experiment efflux curve as well renders the fits a little worse. This indicates that perhaps a minor effect has not entirely been incorporated into the model, but overall it seems that it captures the essence of the interaction of tp10 with phospholipid vesicles. We note that only three rate constants are adjusted by fitting to the CF efflux curves. The fourth constant (k_{eflx}) was fixed because there is a strong correlation between k_{eflx} and k_{dins}. This correlation arises because it is the inserted species that catalyzes efflux, so that the shorter its lifetime the smaller the amount of dye that can escape while the peptide is inserted. Therefore, for sufficiently large values of these two parameters only their ratio, $k_{\mathrm{eflx}}/k_{\mathrm{dins}}$, is significant.

Then, according to the model, what is the reason for the slight difference in CF efflux from POPC and POPS/POPC 2:8? The answer can be obtained by inspecting the behavior of the various tp10 states calculated as a function of time, for the same lipid concentration (20 μM) in POPC (*solid lines*) and POPS/POPC (*dashed lines*), which is shown in Fig. 8. The binding of tp10 to POPC vesicles occurs more slowly

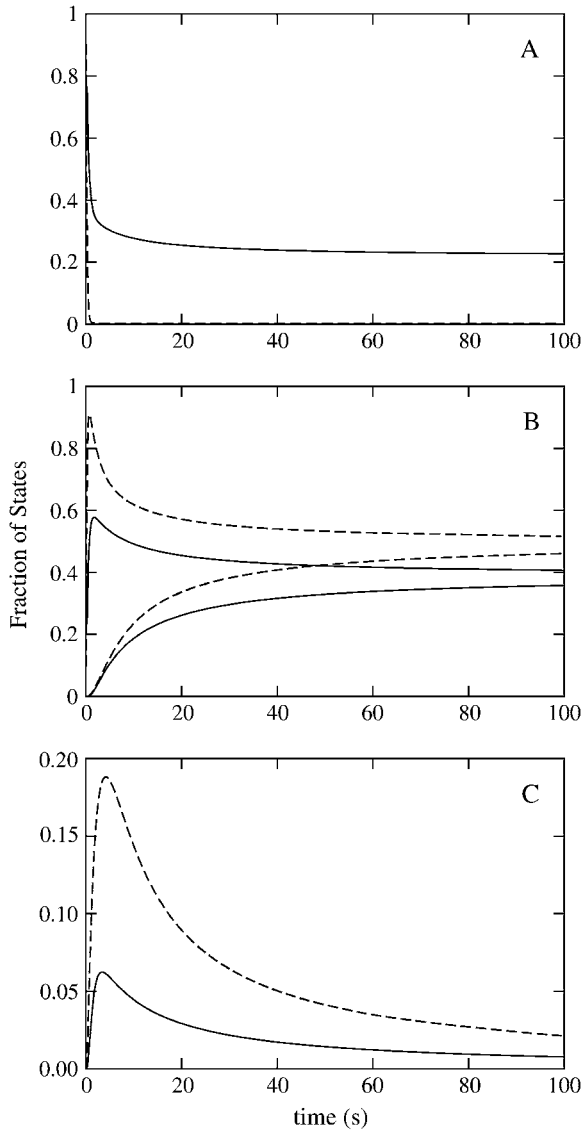

FIGURE 8 The fraction of the different peptide states as a function of time, calculated from the fits for 20 μM POPC (*solid lines*) and 20 μM POPS/POPC 2:8 (*dashed lines*). The tp10 concentration is 0.5 μM in both cases. (*A*) shows the fraction in aqueous solution; (*B*) shows the fraction of tp10 bound to the outer leaflet (*decreasing curves*) and to the inner leaflet (*increasing curves*) of the bilayer; and (*C*) shows the fraction of tp10 inserted into the bilayer. The latter curves should be viewed only qualitatively because of the high degree of correlation between k_{dins} and k_{eflx}, which can significantly alter the time and amplitude of the inserted fractions.

than to POPS/POPC vesicles (Fig. 8 *A*), which is a consequence of the smaller k_{on} in the former. In both cases, the efflux tends to zero as the concentrations of tp10 bound to the outer and inner leaflets of the bilayer approach each other (*B*). The transient of the tp10 concentration in the bilayer (*C*) has a larger amplitude in POPS/POPC 2:8. This is the state that 'catalyzes' efflux; therefore, dye release is a bit faster in POPS/POPC 2:8 than in pure POPC.

DISCUSSION

A detailed investigation of the mechanism of the interaction between the CPP tp10 and phospholipid vesicles was performed. The main finding is that the kinetics of peptide binding to lipid vesicles and the peptide-induced efflux of CF encapsulated in the vesicles are entirely consistent with a very simple model (Fig. 2): first, the peptides bind to the outer surface of the lipid vesicle and their accumulation creates a mass imbalance across the bilayer, which strains the membrane; second, to relieve that perturbation, tp10 monomers translocate across to the inner surface of the membrane. The presence of peptide in the bilayer renders it permeable to the encapsulated dye, which leaks out, concomitant with peptide translocation. When the concentration of tp10 bound to both leaflets of the bilayer is equal, the efflux essentially stops because the mass imbalance strain is relieved and the membrane is no longer perturbed.

The membrane charge plays a significant role in the rates of peptide binding to the membrane surface. As expected, the on-rate to vesicles with a negative charge (POPS/POPC 2:8) is fast, with $k_{on} = 2.6 \times 10^5\ M^{-1}s^{-1}$, essentially diffusion limited, and almost an order of magnitude larger than for zwitterionic vesicles (POPC), with $k_{on} = 7.4 \times 10^4\ M^{-1}s^{-1}$. This, however, is not of much consequence for dye efflux, which occurs at about the same rate from both types of vesicles, because more important than the on-rate is the duration of the membrane perturbation, which is only slightly larger when POPS is present (Fig. 8 *C*).

Tp10 induces dye release in a graded manner. This means that if, at a certain point in time, the mean dye content of the vesicle population is 50% of the initial, all vesicles have released ~50% of their content. The alternative would be an all-or-none mechanism, in which a 50% dye release by the vesicle population would arise from 50% of the vesicles having released all their contents whereas the other 50% released none. The importance of establishing the mechanism of release is that it allows certain models to be discarded. For example, permanent channels, such as the barrel-stave model (29), necessarily produce all-or-none mechanisms and are not consistent with the data for tp10. On the other hand, both the toroidal hole (30,31) and the sinking raft models (17,18) are consistent with a graded mechanism of dye release. Another important model is the carpet model (32,33), in which the peptides first bind to the membrane, oriented parallel to the surface, forming a carpet. At some critical threshold, they cause the vesicle to disintegrate (micellize), releasing all its contents at once. In this extreme case the model is only compatible with all-or-none dye release. Clearly, the action of tp10 is not consistent with this extreme case of the carpet model: there is no threshold, the release is graded, and the concentration of peptide on the vesicle surface in all our experiments is much smaller (peptide/lipid ratio ~1:100) than required to form a complete carpet. However, the carpet model includes the possibility that, at lower peptide surface concentrations, transient pores may form, allowing for graded release of vesicle contents. This may require a high local peptide surface concentration, but not necessarily a coating of the membrane. The model proposed here for the mechanism of tp10 is consistent with this view of the carpet model. Namely, bound peptide is always oriented parallel to the membrane surface, there are no specific tp10 aggregates formed, and dye efflux occurs because of membrane perturbation and not because of a hole 'punched' in the bilayer. Another way of viewing the model presented here is as a limiting case of the sinking raft model, where the 'raft' has only one 'log'.

Most α-helical, amphipathic peptides examined to date are oriented parallel to the membrane surface upon binding, at least at low peptide/lipid ratios (34). This is true, for example, for cecropin A (35,36), LL-37 (37,38), the synthetic antimicrobial peptides MSI-78 and MSI-594, derived from magainin-2 and melittin (39), magainin-2 (40,41), and cecropin-melittin hybrids (42). Some authors have proposed that the peptides insert perpendicular to the bilayer at higher peptide concentrations (30,43), but in most cases this has not been observed. What seems to be emerging is the view that the essential aspect of the activity of these peptides is the perturbation of the membrane, which leads directly to the increase in membrane permeability, for example, to dyes. The notion that large pores are required to achieve this permeability increase is, in our view, incorrect. The concept of large pores developed naturally as an analogy to ion channels (29) but pictured the membrane as a rigid hydrophobic slab into which it was necessary to make a hole to allow water-soluble compounds through. What is missing in that view is the realization that the lipid bilayer properties are not well approximated by an inert hydrophobic slab (23) and that the lipid molecules will adapt to the changes caused by a mass imbalance in the form of bound amphipathic peptides. The concept presented here—that monomers of a 21-residue, amphipathic peptide can permeate the bilayer—may appear unexpected at first. It is, however, well supported by molecular dynamics simulations (20) and thermodynamic analysis using the hydrophobicity scales of White and Wimley (23) for transfer of peptides from water to the bilayer interface and to its interior (mimicked by *n*-octanol), as demonstrated below.

Recent molecular dynamics simulations (20,21) using a coarse-grained representation of lipids and amphipathic antimicrobial polymers indicate that these antimicrobials bind first to the membrane and then cooperatively perturb the

bilayer. As a consequence, the antimicrobials translocate across and water molecules permeate through the bilayer (20). A similar result is shown by all-atom molecular dynamics simulations of a deletion mutant of magainin-2 (22), consistent with what we propose. In our model, the rate of peptide insertion into the hydrophobic core of the bilayer is zero if the membrane is not perturbed. This is, of course, an approximation. But when enough peptides bind to the outer surface of the lipid vesicle, the rate constant for insertion—that is, partition into the hydrophobic core of the bilayer—increases proportionally to the difference in the concentration of peptide bound to the outer and inner leaflets of the membrane, and tp10 readily crosses the bilayer.

Finally, a strong argument in support of the simple model proposed comes from the analysis of the thermodynamics of tp10 association with the membrane and insertion into the bilayer core using the approach of White and Wimley (23). Referring to Fig. 9, let us decompose the process of peptide insertion into the bilayer hydrophobic core into three steps: first, tp10 transfer from water to the bilayer interface; second, folding of tp10 into a helical structure; and third, transfer of tp10 into the bilayer core. Now, using the interfacial scale of White and Wimley (23), the transfer to the interface corresponds to a Gibbs free energy of $\Delta G^{o} = -1.84$ kcal/mol. Helix formation on the membrane/water interface corresponds to $\Delta G^{o} = -6.0$ kcal/mol for a 70% helical structure, which is a typical value for this type of peptide. Transfer of the helix from the surface to the interior can be obtained by completing the thermodynamic cycle with the direct transfer of the helix to the bilayer core. The latter is calculated using the water-octanol hydrophobicity scale (23) and corresponds to $\Delta G^{o} = +11.4$ kcal/mol. Therefore, transfer of tp10 from the membrane surface to its hydrophobic core corresponds to $\Delta G^{o} = +19.8$ kcal/mol. This value should be close to the activation energy ($\Delta G^{\ddagger}$) for bilayer insertion of tp10 from a surface-associated state.

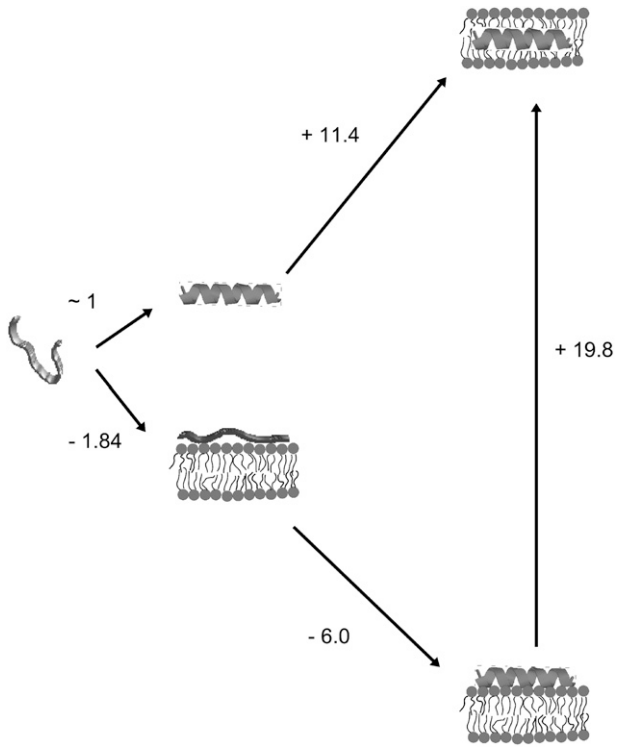

FIGURE 9 Thermodynamic cycle for the transfer of tp10 from water to the bilayer interior. The Gibbs free energies, given in kcal/mol on the figure, were calculated with the program Membrane Protein Explorer (44) (and verified by hand), based on the hydrophobicity scales of White and Wimley (23).

Using 19.8 kcal/mol in the expression for the insertion rate constant, $k = (k_B T/h)\exp(-\Delta G^{\ddagger}/k_B T)$, where k_B is Boltzmann's constant, h is Planck's constant, and T is temperature, a value of $k = 0.013\ s^{-1}$ is obtained. This corresponds to a characteristic time $1/k \sim 80$ s, which is not long and is well within the time frame of the experiments reported here. To compare exactly this value with our insertion rate constant, one must use Eq. 10. Inspection of Fig. 8 *B* shows that the difference between the fraction of tp10 states bound to the outer and inner leaflets of the bilayer varies over the course of the reaction between ~0.8 at the beginning and ~0 at the end. Using ~0.5, a value close to the beginning, in Eq. 10, together with the peptide and lipid concentrations (0.5 and 20 μM), and $k^{*}_{ins} \approx 2\ M^{-1}s^{-1}$ (Table 1), one obtains $k_{ins} \sim 2\ s^{-1}$. This is only 160 times faster than calculated in the absence of any membrane perturbation from the White and Wimley (23) hydrophobicity scales. If a perturbation of the membrane by $\Delta G = +RT\ \ln(160) = 3$ kcal/mol at room temperature is postulated, the calculated rate constant becomes equivalent to the value obtained from the fit. This is a small, entirely plausible perturbation arising from the mass imbalance across the bilayer, caused by peptide binding.

In conclusion, we have proposed a simple model for the mechanism of the interaction of tp10 with lipid vesicles, which involves translocation of the peptide across the membrane. This is not necessarily the only possible model; but it is the simplest model that is entirely consistent with the experimental kinetic data and with the thermodynamics of transfer of tp10 from water to the bilayer interface and to its hydrophobic interior.

We thank Will Boomershine for assistance in the synthesis of the second tp10 batch.

This work was supported in part by National Institutes of Health grant GM072507 (University of North Carolina Wilmington) and by the Swedish Research Council (Stockholm University).

REFERENCES

1. Derossi, D., S. Calvet, A. Trembleau, A. Brunissen, G. Chassaing, and A. Prochiantz. 1996. Cell internalization of the third helix of the Antennapedia homeodomain is receptor-independent. *J. Biol. Chem.* 271:18188–18193.
2. Green, M., and P. M. Lowenstein. 1988. Autonomous functional domains of chemically synthesized human immunodeficiency virus tat trans-activator protein. *Cell.* 55:1179–1188.

3. Frankel, A. D., and C. O. Pabo. 1988. Cellular uptake of the tat protein from human immunodeficiency virus. *Cell.* 55:1189–1193.
4. Soomets, U., M. Lindgren, X. Gallet, M. Hallbrink, A. Elmquist, L. Balaspiri, M. Zorko, M. Pooga, R. Brasseur, and U. Langel. 2000. Deletion analogues of transportan. *Biochim. Biophys. Acta.* 1467:165–176.
5. Hällbrink, M., A. Floren, A. Elmquist, M. Pooga, T. Bartfai, and U. Langel. 2001. Cargo delivery kinetics of cell-penetrating peptides. *Biochim. Biophys. Acta.* 1515:101–109.
6. Zasloff, M. 2002. Antimicrobial peptides of multicellular organisms. *Nature.* 415:389–395.
7. Pooga, M., C. But, M. Kihlmark, M. Hällbrink, S. Fernaeus, R. Raid, T. Land, E. Hallberg, T. Bartfai, and U. Langel. 2001. Cellular translocation of proteins by transportan. *FASEB J.* 15:1451–1453.
8. Magzoub, M., K. Kilk, L. E. G. Eriksson, U. Langel, and A. Gräslund. 2001. Interaction and structure induction of cell-penetrating peptides in the presence of phospholipid vesicles. *Biochim. Biophys. Acta.* 1512: 77–89.
9. Todokoro, Y., I. Yumen, K. Fukushima, S.-W. Kang, J.-S. Park, T. Kohno, K. Wakamatsu, H. Akutsu, and T. Fujiwara. 2006. Structure of tightly membrane-bound mastoparan-X, a G-protein-activating peptide, determined by solid-state NMR. *Biophys. J.* 91:1368–1379.
10. Harada, E., Y. Todokoro, H. Akutsu, and T. Fujiwara. 2006. Detection of peptide-phospholipid interaction sites in bilayer membranes by ^{13}C NMR spectroscopy: observation of $^{2}H/^{31}P$-selective ^{1}H-depolarization under magic-angle spinning. *J. Am. Chem. Soc.* 128: 10654–10655.
11. Hultmark, D., H. Steiner, T. Rasmuson, and H. G. Boman. 1980. Insect immunity. Purification and properties of three inducible bactericidal proteins from hemolymph of immunized pupae of *Hyalophora cecropia*. *Eur. J. Biochem.* 106:7–16.
12. Steiner, H., D. Hultmark, A. Engstrom, H. Bennich, and H. G. Boman. 1981. Sequence and specificity of two antibacterial proteins involved in insect immunity. *Nature.* 292:246–248.
13. Zasloff, M. 1987. Magainins, a class of antimicrobial peptides from Xenopus skin: isolation, characterization of two active forms, and partial cDNA sequence of a precursor. *Proc. Natl. Acad. Sci. USA.* 84: 5449–5453.
14. Mor, A., V. H. Nguyen, A. Delfour, D. Migliore-Samour, and P. Nicolas. 1991. Isolation, amino acid sequence, and synthesis of dermaseptin, a novel antimicrobial peptide of amphibian skin. *Biochemistry.* 30:8824–8830.
15. Caesar, C. E. B., E. K. Esbjörner, P. Lincoln, and B. Nordén. 2006. Membrane interactions of cell-penetrating peptides probed by tryptophan fluorescence and dichroism techniques: correlations of structure to cellular uptake. *Biochemistry.* 45:7682–7692.
16. Sakai, N., T. Takeuchi, S. Futaki, and S. Matile. 2005. Direct observation of anion-mediated translocation of fluorescent oligoarginine carriers into and across bulk liquid and anionic bilayer membranes. *ChemBioChem.* 6:114–122.
17. Pokorny, A., T. H. Birkbeck, and P. F. F. Almeida. 2002. Mechanism and kinetics of δ-lysin interaction with phospholipid vesicles. *Biochemistry.* 41:11044–11056.
18. Pokorny, A., and P. F. F. Almeida. 2004. Kinetics of dye efflux and lipid flip-flop induced by δ-lysin in phosphatidylcholine vesicles and the mechanism of graded release by amphipathic, α-helical peptides. *Biochemistry.* 43:8846–8857.
19. Pokorny, A., and P. F. F. Almeida. 2005. Permeabilization of raft-containing lipid vesicles by δ-lysin: a mechanism for cell sensitivity to cytotoxic peptides. *Biochemistry.* 44:9538–9544.
20. Lopez, C. F., S. O. Nielsen, G. Srinivas, W. F. DeGrado, and M. L. Klein. 2006. Probing membrane insertion activity of antimicrobial polymers via coarse-grain molecular dynamics. *J. Chem. Theory and Comput.* 2:649–655.
21. Nielsen, S. O., C. F. Lopez, G. Srinivas, and M. L. Klein. 2004. Coarse grain models and the computer simulation of soft materials. *J. Phys. Condens. Matter.* 16:R481–R512.
22. Leontiadou, H., A. E. Mark, and S. J. Marrink. 2006. Antimicrobial peptides in action. *J. Amer. Chem. Soc.* 128:12156–12161.
23. White, S. H., and W. C. Wimley. 1999. Membrane protein folding and stability: physical principles. *Annu. Rev. Biophys. Biomol. Struct.* 28: 319–365.
24. Bartlett, G. R. 1959. Phosphorous assay in column chromatography. *J. Biol. Chem.* 234:466–468.
25. Ladokhin, A. S., W. C. Wimley, and S. H. White. 1995. Leakage of membrane vesicle contents: determination of mechanism using fluorescence requenching. *Biophys. J.* 69:1964–1971.
26. Ladokhin, A. S., W. C. Wimley, K. Hristova, and S. H. White. 1997. Mechanism of leakage of contents of membrane vesicles determined by fluorescence requenching. *Methods Enzymol.* 278:474–486.
27. Press, W. H., S. A. Teukolsky, W. T. Vetterling, and B. P. Flannery. 1994. Numerical Recipes in FORTRAN, 2nd ed. Cambridge University Press, New York.
28. Silvestro, L., K. Gupta, J. N. Weiser, and P. H. Axelsen. 1997. The concentration-dependent membrane activity of cecropin A. *Biochemistry.* 36:11452–11460.
29. Ehrenstein, G., and H. Lehar. 1977. Electrically gated ionic channels in lipid bilayers. *Q. Rev. Biophys.* 10:1–34.
30. Ludtke, S. J., K. He, W. T. Heller, T. A. Harroun, L. Yang, and H. W. Huang. 1996. Membrane pores induced by magainin. *Biochemistry.* 35:13723–13728.
31. Matsuzaki, K., O. Murase, N. Fujii, and K. Miyajima. 1996. An antimicrobial peptide, magainin 2, induced rapid flip-flop of phospholipids coupled with pore formation and peptide translocation. *Biochemistry.* 35:11361–11368.
32. Shai, Y. 2002. Mode of action of membrane active antimicrobial peptides. *Biopolymers.* 66:236–248.
33. Papo, N., and Y. Shai. 2003. Can we predict biological activity of antimicrobial peptides from their interactions with model phospholipid membranes? *Peptides.* 24:1693–1703.
34. Bechinger, B. 1999. The structure, dynamics and orientation of antimicrobial peptides in membranes by multidimensional solid-state NMR spectroscopy. *Biochim. Biophys. Acta.* 1462:157–183.
35. Silvestro, L., and P. H. Axelsen. 2000. Membrane-induced folding of cecropin A. *Biophys. J.* 79:1465–1477.
36. Marassi, F. M., S. J. Opella, P. Juvvadi, and R. B. Merrifield. 1999. Orientation of cecropin A helices in phospholipid bilayers determined by solid-state NMR spectroscopy. *Biophys. J.* 77:3152–3155.
37. Oren, Z., J. C. Lerman, G. H. Gudmundsson, B. Agerberth, and Y. Shai. 1999. Structure and organization of the human antimicrobial peptide LL-37 in phospholipid membranes: relevance to the molecular basis for its non-cell-selective activity. *Biochem. J.* 341:501–513.
38. Henzler Wildman, K. A., D.-K. Lee, and A. Ramamoorthy. 2003. Mechanism of lipid bilayer disruption by the human antimicrobial peptide, LL-37. *Biochemistry.* 42:6545–6558.
39. Ramamoorthy, A., S. Thennarasu, D.-K. Lee, A. Tan, and L. Maloy. 2006. Solid-state NMR investigation of the membrane-disrupting mechanism of antimicrobial peptides MSI-78 and MSI-594 derived from magainin 2 and melittin. *Biophys. J.* 91:206–216.
40. Bechinger, B., M. Zasloff, and S. J. Opella. 1992. Structure and interactions of magainin antibiotic peptides in lipid bilayers: a solid-state nuclear magnetic resonance investigation. *Biophys. J.* 62:12–14.
41. Bechinger, B., J.-M. Ruysschaert, and E. Goormaghtigh. 1999. Membrane helix orientation from linear dichroism of infrared attenuated total reflection spectra. *Biophys. J.* 76:552–563.
42. Bhargava, K., and J. B. Feix. 2004. Membrane binding, structure, and localization of cecropin-mellitin hybrid peptides: a site-directed spin-labeling study. *Biophys. J.* 86:329–336.
43. Ludtke, S. J., K. He, and H. W. Huang. 1994. Cooperative membrane insertion of magainin correlated with its cytolytic activity. *Biochim. Biophys. Acta.* 1190:181–184.
44. Membrane Protein Explorer. http://blanco.biomol.uci.edu/mpex/